KELDYSH INSTITUTE OF APPLIED MATHEMATICS
RUSSIAN ACADEMY OF SCIENCES

A.I. Neishtadt, D.J. Scheeres, V.V. Sidorenko,
and A.A. Vasiliev

EVOLUTION OF COMET NUCLEUS ROTATION

MOSCOW
2001

A.I. Neishtadt, D.J. Scheeres, V.V. Sidorenko, A.A. Vasiliev. Evolution of comet nucleus rotation. The secular evolution of comet nucleus rotation states is studied. The dynamical model assumes that the nucleus inertia ellipsoid is axially symmetric and prolate. The outgassing torques acting on the surface are modeled using standard cometary activity formulae. The general rotational equations of motion are derived and separately averaged over the fast rotational dynamics terms and the comet orbit. Special cases where the averaging assumptions cannot be applied are evaluated separately. The modification of the comet orbit due to comet outgassing is neglected. Resulting from this analysis is a system of secular differential equations that describe the dynamics of the comet nucleus angular momentum and rotation state. We find that the qualitative secular evolution of the rotation state is controlled by a single parameter that combines parameters related to the comet orbit and parameters related to the nucleus surface geometry and activity.

А.И.Нейштадт, Д.Дж.Шиерс, В.В.Сидоренко, А.А.Васильев. Эволюция вращения кометного ядра. Изучаются вековые эффекты во вращательном движении кометного ядра. Предполагается, что эллипсоид инерции ядра представляет собой вытянутый эллипсоид вращения. Действие реактивных моментов, возникающих при сублимации кометного вещества под действием солнечной радиации, моделируется в соответствии со стандартными формулами. Выведены общие уравнения вращательного движения ядра. Эти уравнения усредняются по быстрому вращению ядра и по его орбитальному движению. Отдельно рассмотрены случаи, когда такое усреднение неприменимо. Изменением параметров орбиты вследствие испарения кометного вещества пренебрегается. В результате получена система уравнений, описывающая вековые изменения состояния вращения ядра. Показано, что на качественном уровне эволюция вращения ядра определяется единственным параметром, являющимся комбинацией параметров, относящихся к орбите кометы и к геометрии и активности ее ядра.

1.Introduction

Nucleus rotation affects many processes studied in cometary physiscs at a fundamental level [8, 17, 26]. Additionally, hypotheses on likely nucleus rotation states are needed to constrain the mathematical models being developed to simulate and analyse the navigation problems that arise in spacecraft missions to comets [10, 25, 28]. Hence, it is important to understand the long-term dynamics of comet nucleus rotation.

To date there is only limited information on the actual rotation states of active comets. In general, it is possible to evaluate the rotation period of a nucleus using Fourier-analysis of lightcurves [30]. More detailed understanding of the rotation state is possible if the comet has some observable peculiarities such as jets [23]. For several comets, estimated rotation parameters were found using additional assumptions on the properties of nongravitational forces perturbing their orbit motion [29]. In the future, direct observations of comet nuclei by comet-targeted missions will become an important source of information on their rotation. It is these future missions that has motiviated this particular study. Up to now, however, the only precision measurements of comet nucleus rotation that exist are for comet Halley [15, 22].

Reactive torques due to anisotropic sublimation of cometary ice will result in slow variations of a nucleus' rotation parameters. In [12, 21, 24, 31] the spin evolution of comet nuclei was investigated by numerical integration of the equations of nucleus rotation. In the present paper we seek to develop a more systematic approach to the problem by studying the rotational evolution of a cometary nucleus using the averaging method [1, 4]. It will allow us to extract the relevant physical parameters that control the evolution of a comet's rotation state. Additionally, such an approach supplies a general theory that can be used to predict and constrain the rotation states of active and defunct comets.

The averaging method was used in earlier studies of nucleus spin state evolution [13]. However, the model of reactive torque formation assumed in [13] does not take into account more current results and ideas. Thus the averaged equations in [13] cannot be used to study the secular effects found in [21, 24], where sublimation processes are described more realistically. Additionally, in [13] only principal axis rotation states were considered, while in the current analysis we consider the space of all possible rotations.

2.Model Description

Main assumptions. We assume that the comet moves along an elliptic orbit with an eccentricity e and a perihelion distance r_π. The effects of comet outgassing on the evolution of the orbit are beyond the scope of this paper.

We consider the comet nucleus to be a solid object which can be studied using the methods of rigid body dynamics. We also suppose that nucleus is mostly prolate [11, 20], and that its shape is approximated by polyhedron (for example, using a triangulation methods [16]).

One of the stronger assumptions that we make is that the principal moments of inertia of the nucleus A_*, B_*, C_* satisfy the condition

$$A_* = B_* > C_* . \tag{1}$$

Estimates of the principal moments of inertia derived from measurements of comet nuclei using various methods [15, 19] show that the corresponding ellipsoids of inertia appear to be nearly axially symmetric. In future work, we plan to also consider the general, non-symmetric case. As our analysis considers time periods on the order of several tens or hundreds of comet apparitions, we neglect the possible effects due to variation of the nucleus shape and its moments of inertia, following [21, 24].

To calculate the reactive torque acting on a comet nucleus due to anisotropic sublimation we use the formula

$$\mathbf{M} = -\sum_{j=1}^{N} Q_j(\mathbf{R}_{*j} \times \mathbf{v}_j) , \tag{2}$$

where N is the number of faces of the polyhedron that approximates the nucleus shape, Q_j is the mass ejection rate on the j-th face, $\mathbf{R}_{*j}$ is the radius vector of the face's center in the body's principal frame of reference, and $\mathbf{v}_j$ is the effective velocity of the ejected matter.

In [21, 24] it was assumed that active mass ejection takes place only on several relatively small parts of the surface, forming narrow jets. Such jets can be seen on pictures of the Halley comet nucleus [15]. In more recent studies [6], jets were considered as a manifestation of the nonhomogeneity of gas and dust flows in comet atmospheres, mostly resulting from the topography of the nucleus rather than from differences in physical properties of its surface. The model and analysis we use here can be applied to both of these extreme cases, and all others that lie between them. The current formulation does assume that the nucleus shape is described by a convex body – another strong assumption that will be studied more closely in the future.

In simple models of the sublimation process, the mass ejection rate is determined by the heliocentric distance to the comet and by the local solar insolation:

$$Q_j = s_j f(\delta_j) g(r) Q_* \,. \tag{3}$$

Here Q_* is the mass ejection rate from a plane surface with an area equal to the total surface area of the nucleus, oriented perpendicularly to the direction to the Sun at a heliocentric distance of 1 AU, s_j is the relative intensity (the ratio of the maximal possible mass ejection rate from the j-th face at this heliocentric distance to Q_*), δ_j is the angle between the outer normal of the j-th face ($\mathbf{n}_j$) and the unit vector pointing to the Sun ($\mathbf{e}_s$), and r is the heliocentric distance.

An empirical expression for $g(r)$, suggested in [18], is

$$g(r) = g_0 \left(\frac{r}{r_0}\right)^{-c_1} \left[1 + \left(\frac{r}{r_0}\right)^{c_2}\right]^{-c_3} , \tag{4}$$

where

$$c_1 = 2.15,\ c_2 = 5.093,\ c_3 = 4.6142,\ r_0 = 2.808,\ g_0 = 0.111262.$$

This expression has been used to describe nongravitational perturbations in numerous papers (see, for example [8, 17]). One should note that Eq. 4 does not account for the observed asymmetry of comet activity with respect to perihelion passage [32]. However, it will be shown in Appendix A that under acceptable assumptions about sublimation processes this asymmetry does not change the nucleus spin evolution dramatically.

The function $f(\delta_j)$ defines the dependence of the mass ejection rate on the angle between the direction to the Sun and the normal to the j-th face. A variety of realizations of this function can be made. For example, in [24, 31], the hypothesis is made that the mass ejection rate on non-illuminated faces is zero, leading to a functional form:

$$f(\delta_j) = \begin{cases} \cos\delta_j = (\mathbf{e}_s, \mathbf{n}_j), & \delta_j \le \frac{\pi}{2} \\ 0\,, & \delta_j > \frac{\pi}{2} \end{cases} \tag{5}$$

In this paper, we use the empirical formula that takes into account the dependence of mass ejection on heat transfer in the external layer of the nucleus [28]:

$$f(\delta_j) = 1 - \alpha(1 - \cos\delta_j), \quad 0 < \alpha \le \frac{1}{2}\,. \tag{6}$$

The magnitude of the reactive torque in Eq. 2 rapidly decreases as the cometary solar distance grows (as $\sim r^{-25.7}$). Nevertheless, we consider the reactive

torques as the only factor changing the nucleus rotation state. This approach is quite traditional in studies of spin evolution of short-period comets, with periods of rotation around the Sun $T < 200$ years [21, 24, 31]. For long-period comets, which spend a long time on the periphery of the Solar system, the effects of energy dissipation due to nonstationary deformations of the rotating nuclei by inertia forces become more significant [5, 7].

Coordinate frame definitions. To describe the rotation of the comet nucleus, we introduce three right-hand orthogonal coordinate systems with their origin at the nucleus center of mass:

$OXYZ$: The "perihelion" system, with the OZ-axis parallel to the Sun-perihelion line, the OY-axis normal to the plane of the orbit, and the OX-axis parallel to the tangent to the orbit at perihelion and pointing in the direction of orbit motion;

$Oxyz$: The frame connected with the angular momentum vector of the nucleus $\mathbf{L}$. The Oz axis is directed along $\mathbf{L}$, the Oy axis is in the plane OXY, and the Ox axis follows from the right-hand rule;

$O\xi\eta\zeta$: The body-fixed system, the axes $O\xi$, $O\eta$, $O\zeta$ being aligned with the principal axes of inertia.

We define the orientation of the coordinate systems $Oxyz$ with respect to the "perihelion"system $OXYZ$ with the angles ρ (the cone angle) and σ (the clock angle), shown in Fig. 1. A turn through angle σ around the OZ axis followed by a turn through angle ρ around the Oy axis rotates the trihedron $Oxyz$ into its current position starting from an initial orientation with the Ox, Oy, Oz axes coinciding with the axes OX, OY, OZ. The corresponding matrix has the form:

	x	y	z
X	m_{Xx}	m_{Xy}	m_{Xz}
Y	m_{Yx}	m_{Yy}	m_{Yz}
Z	m_{Zx}	m_{Zy}	m_{Zz}

$$m_{Xx} = \cos\sigma\cos\rho \qquad m_{Xy} = -\sin\sigma \qquad m_{Xz} = \cos\sigma\sin\rho$$

$$m_{Yx} = \sin\sigma\cos\rho \qquad m_{Yy} = \cos\sigma \qquad m_{Yz} = \sin\sigma\sin\rho$$

$$m_{Zx} = -\sin\rho \qquad m_{Zy} = 0 \qquad m_{Zz} = \cos\rho$$

We define the orientation of the system $O\xi\eta\zeta$ with respect to the system $Oxyz$ by the Euler angles ψ, ϑ, φ. Of particular interest is the angle ϑ (the nutation angle) corresponding to the angle between the angular momentum vector and the long axis of the inertia ellipsoid. The matrix in this case is

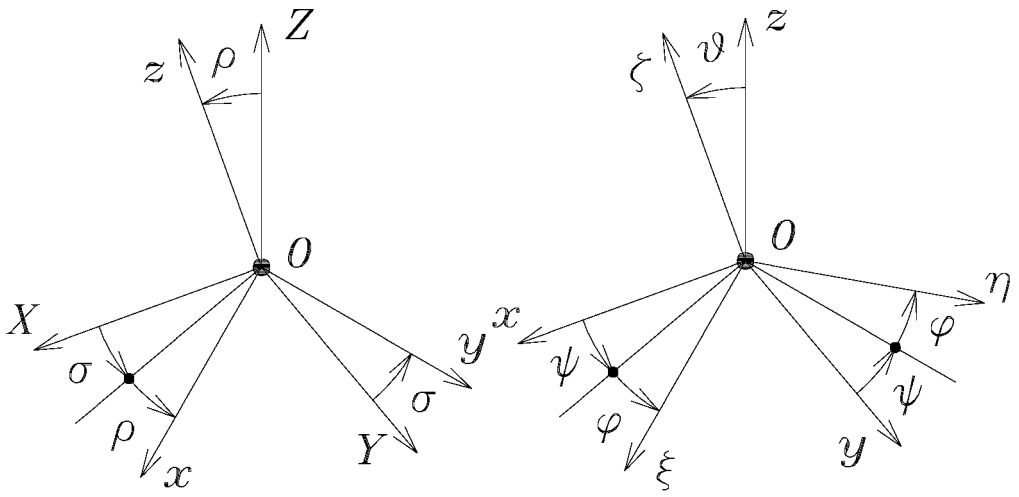

Fig.1. Angles and coordinate systems used to describe the comet nucleus motion.

	ξ	η	ζ
x	$a_{x\xi}$	$a_{x\eta}$	$a_{x\zeta}$
y	$a_{y\xi}$	$a_{y\eta}$	$a_{y\zeta}$
z	$a_{z\xi}$	$a_{z\eta}$	$a_{z\zeta}$

$$a_{x\xi} = \cos\psi\cos\varphi - \sin\psi\sin\varphi\cos\vartheta$$
$$a_{y\xi} = \sin\psi\cos\varphi + \cos\psi\sin\varphi\cos\vartheta$$
$$a_{z\xi} = \sin\varphi\sin\vartheta$$

$$a_{x\eta} = -\cos\psi\sin\varphi - \sin\psi\cos\varphi\cos\vartheta$$
$$a_{y\eta} = -\sin\psi\sin\varphi + \cos\psi\cos\varphi\cos\vartheta$$
$$a_{z\eta} = \sin\vartheta\cos\varphi$$

$$a_{x\zeta} = \sin\vartheta\sin\psi$$
$$a_{y\zeta} = -\sin\vartheta\cos\psi$$
$$a_{z\zeta} = \cos\vartheta$$

3.Dynamical Model and Averaging Approximations

Equations of motion. The complete set of equations for rotational motion consists of a set of equations describing its rotation in the coordinate system $Oxyz$ and a set of equations for the time evolution of its angular momentum vector.

It is convenient to use dimensionless variables and parameters in the equations of motion. Take as an independent variable $\tau_* = \Omega_* t$, where Ω_* is a typical value of the nucleus initial angular velocity. The values of the parameters A and C specified below are equal to the ratios of the equatorial and axial moments of inertia A_* and C_* with $I_* = m_* R_*^2$, where m_* is the nucleus mass and R_* is its mean radius. The dimensionless variable L is the ratio of the magnitude of the angular momentum vector to $L_* = I_* \Omega_*^2$. Components of the vectors $\mathbf{R}_j$ given below are components of $\mathbf{R}_{*j}$ in Eq. 2 divided by R_*.

Taking into account the assumptions made above, the equations of motion can be written in the following form [3]:

$$\begin{aligned}
\frac{d\vartheta}{d\tau} &= \frac{1}{L}\left[(M_\xi \sin\varphi + M_\eta \cos\varphi)\cos\vartheta - M_\zeta \sin\vartheta\right], \\
\frac{d\psi}{d\tau} &= \frac{L}{A} - \frac{M_x}{L}\cos\psi\cot\vartheta - \frac{M_y}{L}(\cot\rho + \sin\psi\cot\vartheta), \\
\frac{d\varphi}{d\tau} &= L\cos\vartheta\left(\frac{1}{C} - \frac{1}{A}\right) + \frac{M_\xi\cos\varphi - M_\eta\sin\varphi}{L\sin\vartheta}, \\
\frac{d\rho}{d\tau} &= \frac{M_x}{L}, \quad \frac{d\sigma}{d\tau} = \frac{M_y}{L\sin\rho}, \quad \frac{dL}{d\tau} = M_z,
\end{aligned} \tag{7}$$

where

$$M_{x(y,z)} = a_{x(y,z)\xi} M_\xi + a_{x(y,z)\eta} M_\eta + a_{x(y,z)\zeta} M_\zeta \,,$$

$$M_{\xi(\eta,\zeta)} = \varepsilon g(r) \sum_{j=1}^{N} s_j d_{j\xi(\eta,\zeta)} [(1-\alpha) + \alpha(\mathbf{e}_s, \mathbf{n}_j)] \,,$$

$$d_{j\xi} = n_{j\eta} R_{j\zeta} - n_{j\zeta} R_{j\eta} \,, \; d_{j\eta} = n_{j\zeta} R_{j\xi} - n_{j\xi} R_{j\zeta} \,,$$

$$d_{j\zeta} = n_{j\xi} R_{j\eta} - n_{j\eta} R_{j\xi} \,,$$

and

$$\varepsilon = \frac{v_* Q_* R_*}{I_* \Omega_*^2} \,. \tag{8}$$

Here v_* is the velocity of ejected matter and the values M_x, M_y, M_z and M_ξ, M_η, M_ζ in Eqs. 7 are the projections of reactive torques onto the corresponding axes in the coordinate systems $Oxyz$ and $O\xi\eta\zeta$.

The parameter ε determines the overall influence of the reactive torques on the nucleus. In Table I, estimates of this parameter for several comets are presented (we assume the velocity of ejected matter to be $v_* = 0.25 \frac{km}{sec}$).

Table I.Typical parameter values derived from published data [12, 14].

Comet name	$Q_*\left(\frac{kg}{hr}\right)$	$R_*(km)$	$m_* \cdot 10^{-12}$ (kg)	$I_* \cdot 10^{-12}$ $(kg \cdot km^2)$	Ω_* (hr^{-1})	ε
			Jupiter comets			
2P/Encke	$5.1 \cdot 10^7$	2.3	53.7	294	0.97	$9.4 \cdot 10^{-4}$
46P/Wirtanen	$3.4 \cdot 10^6$	0.6	0.9	0.32	1	$5.7 \cdot 10^{-3}$
			Neptune comets			
1P/Halley	$2.3 \cdot 10^8$	5	525	13100	0.1	$7.9 \cdot 10^{-3}$
109P/Swift-Tuttle	$1.3 \cdot 10^9$	12	7240	10^6	0.1	$1.4 \cdot 10^{-3}$

For $\varepsilon = 0$ (an "old" comet without any signs of activity) Eqs. 7 can be easily integrated:

$$\psi = \omega_\psi \tau + \psi_0 \,, \;\; \varphi = \omega_\phi \tau + \varphi_0 \,,$$
$$\vartheta = \vartheta_0 \,, \;\; \rho = \rho_0 \,, \;\; \sigma = \sigma_0 \,, \;\; L = L_0 \,. \qquad (9)$$

Here

$$\omega_\psi = \frac{L}{A} \,, \;\; \omega_\varphi = L \cos\vartheta \left(\frac{1}{C} - \frac{1}{A} \right) \,.$$

The motion in this case is a regular precession: the longest axis of the nucleus (more precisely, the symmetry axis of its inertia ellipsoid) rotates at a constant angular velocity ω_ψ around the angular momentum vector, forming a constant angle ϑ. The nucleus itself rotates around its longest axis at a constant angular velocity ω_φ.

If $\varepsilon \ll 1$, the nucleus motion can be considered to be a perturbed regular precession: the precession parameters, direction and magnitude of the angular momentum vector are slowly changing under the action of the reactive torque ($\frac{d\vartheta}{d\tau}, \frac{d\rho}{d\tau}, \frac{d\sigma}{d\tau}, \frac{dL}{d\tau} \sim \varepsilon$). The averaging method [1, 4] can be used to study the behavior of the slow variables $\vartheta, \rho, \sigma, L$ over long time scales (on the order of $\sim \varepsilon^{-1}$).

An important property of the Eqs. 7 should be noted: if

$$(\vartheta(\tau), \rho(\tau), \sigma(\tau), L(\tau), \varphi(\tau), \psi(\tau))$$

is a solution of the system, then

$$(\pi - \vartheta(-\tau), \pi - \rho(-\tau), \pi + \sigma(-\tau), L(-\tau), \pi + \varphi(-\tau), \pi - \psi(-\tau))$$

is also a solution. This "reversibility" of solutions is due to absence of dissipation in our force model for the comet nucleus dynamics. Also, it should be noted that the variables $\vartheta, \psi, \varphi, \rho, \sigma, L$ are noncanonically modified Andoyer variables, previously used to study the rotation of comet nuclei in [27].

First-order equations of the averaging method. Evolution of the slow variables. We will perform the averaging in two steps: first we average over the nonperturbed nucleus motion and second over the nucleus motion along its heliocentric orbit. These separate averagings are possible because of the large differences between $\omega_\varphi, \omega_\psi$ and the comet mean motion $\Omega_0 = 2\pi/T$, where in general $\omega_\varphi \sim \omega_\psi \gg \Omega_0$.

Averaging over the motion (9) is equivalent to the change of variables (close to the identity transformation)

$$\vartheta = \overline{\vartheta} + O(\varepsilon), \;\; \rho = \overline{\rho} + O(\varepsilon), \;\; \sigma = \overline{\sigma} + O(\varepsilon), \;\; L = \overline{L} + O(\varepsilon), \qquad (10)$$

which permits us to transform the original equations for the slow variables to equations with a r.h.s. that does not depend on φ and ψ:

$$\frac{d\overline{\vartheta}}{d\tau} = \varepsilon H_\vartheta(\overline{\vartheta},\overline{\rho},\overline{\sigma},\overline{L},\nu)\,,\ \frac{d\overline{\rho}}{d\tau} = \varepsilon H_\rho(\overline{\vartheta},\overline{\rho},\overline{\sigma},\overline{L},\nu)\,, \tag{11}$$
$$\frac{d\overline{\sigma}}{d\tau} = \varepsilon H_\sigma(\overline{\vartheta},\overline{\rho},\overline{\sigma},\overline{L},\nu)\,,\ \frac{d\overline{L}}{d\tau} = \varepsilon H_L(\overline{\vartheta},\overline{\rho},\overline{\sigma},\overline{L},\nu)\,.$$

In the first order approximation of the averaging method we find

$$H_\vartheta = \frac{g(r(\nu))\sin\vartheta}{2L}[3\alpha D_1\cos\vartheta(m_{Xz}\sin\nu + m_{Zz}\cos\nu) - 2(1-\alpha)D_0]\,,$$
$$H_\rho = \frac{\alpha g(r(\nu))}{2L}[D_2 m_{Xy}\cos\vartheta\sin\nu + D_1 R(\vartheta)(m_{Xx}\sin\nu + m_{Zx}\cos\nu)]\,,$$
$$H_\sigma = \frac{\alpha g(r(\nu))}{2L\sin\rho}[D_1 R(\vartheta)m_{Xy}\sin\nu - D_2(m_{Xx}\sin\nu + m_{Zx}\cos\nu)\cos\vartheta]\,,$$
$$H_L = -g(r(\nu))[\alpha D_1 R(\vartheta)(m_{Xz}\sin\nu + m_{Zz}\ cos\nu) - (1-\alpha)D_0\cos\vartheta]\,,$$

where $\nu = \nu(\tau)$ is the true anomaly, and

$$R(\vartheta) = \frac{1}{2}(2 - 3\sin^2\vartheta)\,,\ D_0 = \sum_{j=1}^{N} s_j d_{j\zeta}\,,$$
$$D_1 = \sum_{j=1}^{N} s_j d_{j\zeta} n_{j\zeta}\,,\ D_2 = \sum_{j=1}^{N} s_j (d_{j\eta} n_{j\xi} - d_{j\xi} n_{j\eta}).$$

If the condition

$$n\omega_\psi = m\omega_\phi\ (m = 1,2; n = 0,\pm1,\pm2) \tag{12}$$

holds, the averaging change of variables (10) does not exist and a special analysis must be performed. Equation 12 defines a family of resonant hyperplanes in the space of $(\vartheta,\rho,\sigma,L)$:

$$\cos\vartheta = 0,\ \cos\vartheta = \pm\frac{C}{2(A-C)} \quad (\text{if } 2A > 3C),$$

$$\cos\vartheta = \pm\frac{C}{(A-C)} \quad (\text{if } A > 2C),$$

$$\cos\vartheta = \pm\frac{2C}{(A-C)} \quad (\text{if } A > 3C).$$

The second step of our averaging procedure is to average over the orbital motion. To do this, introduce new variables $\overline{\vartheta}, \overline{\rho}, \overline{\sigma}, \overline{L}$ describing the secular component in the variation of the rotation parameters. Such an averaging makes sense if these parameters change only a little during one orbit of the comet around the Sun.

After averaging over the orbital motion, Eqs. 11 take the form (using the original notations for the doubly-averaged variables):

$$\frac{d\vartheta}{d\tau} = \frac{\varepsilon}{2L}[3\alpha D_1\Phi_1 \cos\rho\cos\vartheta - 2(1-\alpha)D_0\Phi_0]\sin\vartheta\,, \tag{13}$$

$$\frac{d\rho}{d\tau} = -\frac{\varepsilon\alpha\sin\rho}{4L}(2-3\sin^2\vartheta)D_1\Phi_1\,, \frac{d\sigma}{d\tau} = \frac{\varepsilon\alpha}{2L}\cos\vartheta D_2\Phi_1\,,$$

$$\frac{dL}{d\tau} = -\frac{\varepsilon}{2}[\alpha D_1\Phi_1(2-3\sin^2\vartheta)\cos\vartheta - 2(1-\alpha)D_0\Phi_0\cos\vartheta]\,.$$

Here

$$\Phi_0 = \frac{(1-e^2)^{3/2}}{\pi}\int_0^\pi \frac{g(r(\nu))d\nu}{(1+e\cos\nu)^2}\,, \tag{14}$$

$$\Phi_1 = \frac{(1-e^2)^{3/2}}{\pi}\int_0^\pi \frac{\cos\nu g(r(\nu))d\nu}{(1+e\cos\nu)^2}\,.$$

One can consider the condition

$$\varepsilon_* = \varepsilon\Phi_0\left(\frac{\Omega_*}{\Omega_0}\right) \ll 1. \tag{15}$$

as a formal criterion of the appliability for averaging over the orbital motion. The comets listed in Table I, do not meet the condition (15): for all of them we have $\varepsilon_* \sim 1$. However, one should note that the parameter ε gives an excessive estimate of the effect of reactive torques on the nucleus rotation. Results of computer integrations show that even at $\varepsilon_* \sim 1$ the averaged equations give a good description of a nucleus spin evolution, provided that the active zones are distributed realistically.

Initial nucleus motion. In this study we assume that the influence of reactive torques on the nucleus dynamics dominates its rotational evolution. This hypothesis, however, does not exclude the possibility that other physical processes may result in certain specific modes of initial nucleus rotation. In [21, 24], it was assumed that comet nuclei are initially rotating in a relaxed

configuration, with their long axis perpendicular to the angular momentum vector ($\vartheta \approx \frac{\pi}{2}$). Such a mode should be typical for a comet from the Oort cloud after its transition to a short-period orbit (perhaps as a result of a close flyby of one of the big planets). Indeed, when the comet is far from the Sun, dissipation caused by deformations due to inertia forces would result in a decrease in the kinetic energy while the angular momentum holds constant. If $\vartheta \approx \frac{\pi}{2}$, the resonance $\omega_\varphi \approx 0$ takes place in the nucleus attitude motion. The conditions for capture into the resonance $\omega_\varphi \approx 0$ are given in Appendix B (in particular, such a capture is impossible if the mass ejection is localized at one small region on the nucleus surface). It is important to note that even in the absence of reactive torques ($\varepsilon = 0$) the general properties of motion at $\vartheta \approx \frac{\pi}{2}$ change dramatically if nucleus inertia ellipsoid is not axially symmetric. Therefore we will not investigate the details of the evolution near $\vartheta \approx \frac{\pi}{2}$ in the current paper – it is more reasonable to do so under the assumption that the main axes of the inertia ellipsoid are different (as mentioned in Sect.1, we will consider this case in the future).

In any case, the averaged equations (13) adequately describe the evolution of most of the "non-resonant" initial values of phase variables lying outside the small vicinity of the resonance hyperplanes. The capture of a nucleus rotation state in one of the resonances in Eq. 12 will be a low-probability event in general.

4.Solutions of the averaged equations. Secular effects.

Analysis of the averaged equations (13) can establish some qualitative properties of the evolution of cometary nucleus rotation. An important property of (13) is the independence of the r.h.s. from the variable σ (a consequence of the implied symmetry of the system before and after perihelion passage). Thus, we can analyse the closed subsystem describing the evolution of the total angular momentum L, the nutation angle ϑ, and the cone angle ρ of the angular momentum vector.

Evolution of the rotation state and orientation. Moreover, if we take as an independent variable

$$\tau_* = \frac{1}{\Phi_1} \int_0^\tau \frac{d\tau'}{L} \tag{16}$$

we obtain a closed subsystem for ϑ and ρ:

$$\frac{d\rho}{d\tau_*} = -\frac{\varepsilon \alpha D_1}{4} \sin\rho (2 - 3\sin^2\vartheta)\,, \tag{17}$$

$$\frac{d\vartheta}{d\tau_*} = \frac{\varepsilon D_1}{2}[3\alpha\cos\rho\cos\vartheta - 2(1-\alpha)\kappa]\sin\vartheta\,,$$

where

$$\kappa = \frac{D_0\Phi_0}{D_1\Phi_1}. \tag{18}$$

If $|\kappa| > \kappa_1 = \frac{3\alpha}{2(1-\alpha)}$, the stationary points of Eqs. 17 lie at the vertices of the square $\mathcal{K} = \{0 \le \rho \le \pi, 0 \le \vartheta \le \pi\}$, labeled as K_1, K_2, K_3, K_4. One of these vertices is a stable node, the opposite one is an unstable node, and the other two are saddles. The phase portrait shown in Fig.2a represents the typical behavior of solutions of Eqs 17 at $|\kappa| > \kappa_1$. For definiteness, here and below we consider the dynamics for positive values of D_1 and non-negative values of κ; if $D_1 < 0$, the motion on the phase trajectories is directed backwards; phase portraits at negative values of κ are obtained by reflection with respect to the line $\rho = \pi/2$.

Based on the phase portrait in Fig.2a one can conclude that at $\kappa > \kappa_1$, and for arbitrary initial conditions, the effects of the reactive torque (2) results in the monotonic decrease of the nutation angle ϑ, causing the nucleus to eventually spin about its minimum moment of inertia. The angle between the angular momentum vector $\mathbf{L}$ and the perihelion radius vector will decrease if $\vartheta < \arccos\frac{1}{\sqrt{3}}$ and $\vartheta > \pi - \arccos\frac{1}{\sqrt{3}}$, at other values of ϑ this angle will increase. The stable stationary point corresponds to $\mathbf{L}$ and the $O\zeta$ axis being directed along the radius vector of the perihelion, for motion attracted to the stable node these vectors will align with the perihelion radius vector as time grows large.

At $\kappa = \kappa_1$ a bifurcation occurs, producing inside of the square $\mathcal{K}$ two new stationary points

$$M_1 = \left(0, \arccos\frac{2(1-\alpha)\kappa}{3\alpha}\right),\ M_2 = \left(\pi, \pi - \arccos\frac{2(1-\alpha)\kappa}{3\alpha}\right). \tag{19}$$

The phase portrait of the system of Eqs. 17 at $\kappa_1 > \kappa > \kappa_2 = \frac{\kappa_1}{\sqrt{3}}$ is shown in Fig. 2b. In the limit motion, corresponding to the only stable stationary point (either M_1 or M_2, depending on the values of D_1 and κ), the nucleus precesses around the angular momentum vector directed in the direction of the perihelion vector.

The bifurcation at $\kappa = \kappa_2$ produces the additional stationary points

$$N_1 = \left(\arccos\frac{2(1-\alpha)\kappa}{\sqrt{3}\alpha}, \arccos\frac{1}{\sqrt{3}}\right), \tag{20}$$

$$N_2 = \left(\pi - \arccos\frac{2(1-\alpha)\kappa}{\sqrt{3}\alpha}, \pi - \arccos\frac{1}{\sqrt{3}}\right). \tag{21}$$

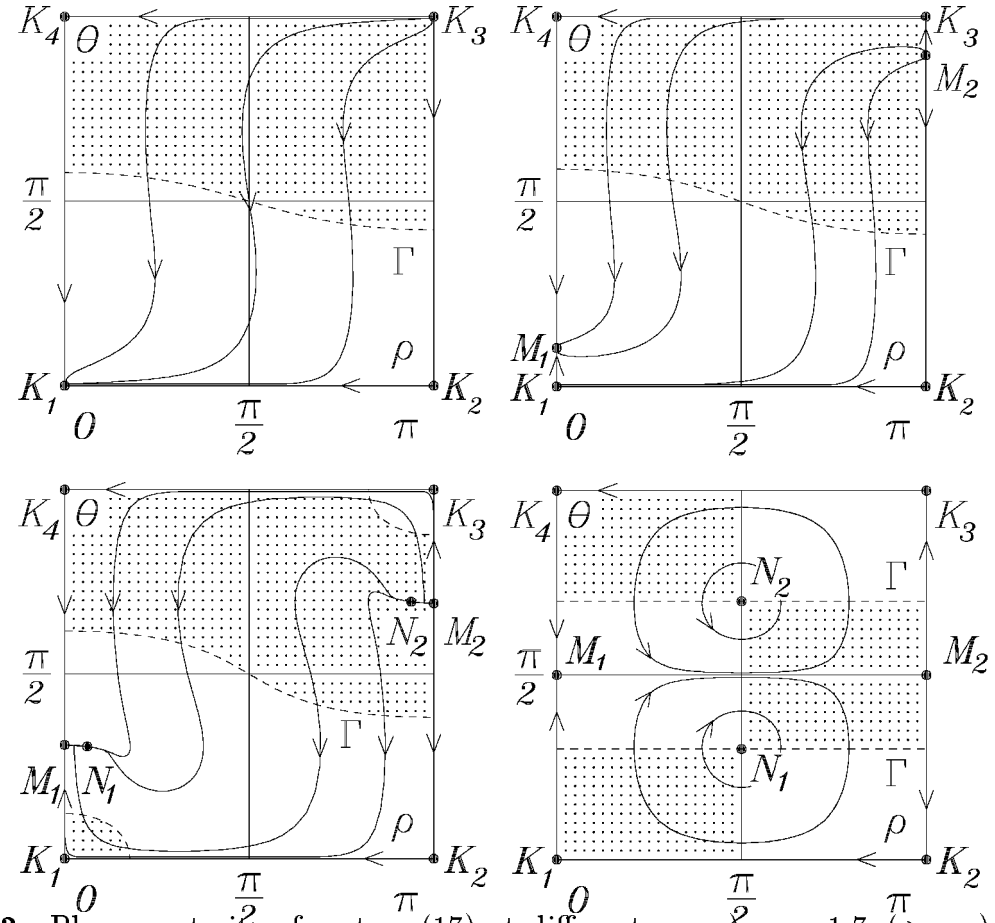

Fig.2. Phase portraits of system (17) at different κ: a) $\kappa = 1.7$ $(> \kappa_1)$, b) $\kappa = 1.42$ $(\in (\kappa_1, \kappa_2))$, c) $\kappa = 0.85$ $(\in (\kappa_2, \kappa_3))$, d) $\kappa = 0$. In all cases $D_1 > 0$, $\alpha = 0.5$.

The phase portrait of the system of Eqs. 17 at $\kappa_2 > \kappa > \kappa_3 = \kappa_1\sqrt{2}/3$ is shown in Fig. 2c. In this case the evolved direction of the angular momentum vector differs from the perihelion vector, and the nucleus evolves to a nutation angle of $\sim 55^\circ$ in general.

At $\kappa = \kappa_3$ the type of the stationary points N_1 and N_2 change. For $\kappa_3 > \kappa > 0$ they become foci, while for $\kappa > \kappa_3$ they were simple hyperbolic points.

In the degenerate case of $\kappa = 0$ the points N_1 and N_2 become stable centers. The corresponding phase portrait is shown in Fig. 2d.

The reversibility of the equations of motion, noted in Section 3, results in a symmetry of the phase portraits: they are invariant with respect to change of directions of the arrows followed by the rotation mapping $K_1 \to K_3, K_2 \to K_4, K_3 \to K_1, K_4 \to K_2$.

Angular momentum. Now consider the nucleus angular momentum. The r.h.s. of the last equation of system (13) is zero on a curve Γ defined in $\mathcal{K}$ (see Fig.2). This curve, together with the sides of the square, bound the areas where the magnitude of the angular momentum grows and where it diminishes (on the phase portraits the areas where the magnitude of the angular momentum diminishes are shaded). At $\kappa \geq \kappa_4 = \frac{\alpha}{1-\alpha}$ the curve Γ divides $\mathcal{K}$ into two parts; at $\kappa_4 > \kappa \neq 0$ the curve consists of three segments and divides $\mathcal{K}$ into four parts, as shown in Fig. 2c; the case $\kappa = 0$ is shown in Fig. 2d.

In the nondegenerate case $(\kappa \neq 0)$ in the limit as $\tau \to +\infty$, the angular momentum will grow as $L \sim \varepsilon c_0 \tau$, where c_0 can be found after substituting into the third equation of the averaged system $\vartheta_0 = \lim_{\tau\to+\infty} \vartheta(\tau)$ and $\rho_0 = \lim_{\tau\to+\infty} \rho(\tau)$. For the case of $\kappa = 0$ the angular momentum will go through periods of increasing and decreasing magnitude.

We conclude the qualitative analysis of evolution of the nucleus rotation parameters with a brief remark on the evolution of the angular momentum clock angle σ. It follows from the corresponding equations of system (13) that σ evolves in opposite directions according to whether $\vartheta < \frac{\pi}{2}$ or $\vartheta > \frac{\pi}{2}$. Hence, if the initial conditions do not allow nucleus rotation around its short axis during a certain stage of the evolution, the angle σ during this stage will either monotonically increase or decrease.

Resonant motion. The averaged equations (13), formally extended onto all the phase space $(\vartheta, \rho, \sigma, L)$, describe the nucleus spin evolution at $\varepsilon \ll 1$ for a majority of initial conditions [2]. However, these equations cannot be used if large regions of the phase trajectories lie in the vicinity of one of the hypersurfaces (12). Such motions are resonant and will preserve, for a long time, a relation of the form

$$n\omega_\psi \approx m\omega_\phi \ (m = 1, 2; n = 0, \pm 1, \pm 2). \tag{22}$$

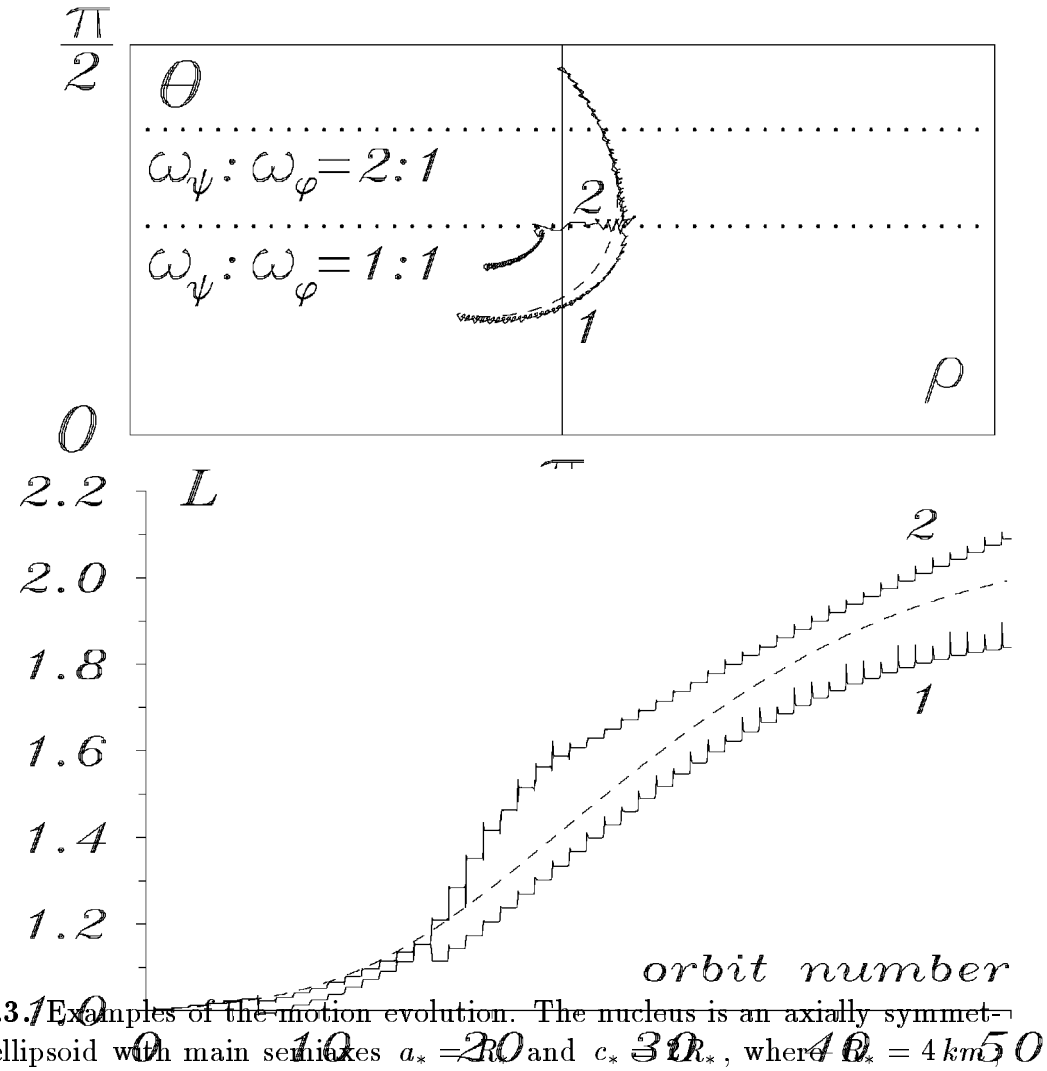

Fig.3.1 Examples of the motion evolution. The nucleus is an axially symmetric ellipsoid with main semiaxes $a_* = 2R_*$ and $c_* = 3R_*$, where $R_* = 4\,km$; its total mass is $m_* = 6.25 \cdot 10^{13} kg$. Identical active zones are placed not far from poles: $\mathbf{R}_1 = (0.3326, 0, 1.8861)R_*$, $\mathbf{R}_2 = (0.302, 0, -1.9066)R_*$, the jet directions are close to the external normals to the surface: $\mathbf{n}_1 = (0.55, -0.1724, 0.8172)$, $\mathbf{n}_2 = (0.5107, 0.1600, -0.8447)$. The sublimation model parameters are: $\alpha = 0.5$, $v_* = 250\,m/cek$, $Q_* = 2.02 \cdot 10^8\,kg/hr$ ($\varepsilon = 1.8 \cdot 10^{-3}$). Initial magnitude of the angular momentum is $6.25 \cdot 10^{16}\,kg \cdot m^3/sek$ ($\Omega_* = 0.9\,hr^{-1}$), the angular momentum vector is normal to the orbital plane ($\rho(0) = \sigma(0) = 90^o$). The large axis of the nucleus in the initial precession is at the angle $\vartheta(0) = 85^o$ from it. Motions 1 and 2 have at $\tau = 0$ different values of the angle φ ($\varphi(0) = 120^o$ and $\varphi(0) = 85^o$), the precession angle $\psi(0) = 0^o$. The dashed line corresponds to the solution of the averaged equations with above mentioned initial conditions $\vartheta(0), \rho(0), \sigma(0)$ and $L(0) = 1$. Parameters in (13) are: $D_0 = 4.5 \cdot 10^{-3}$, $D_1 = 4.383 \cdot 10^{-2}$, $D_2 = -3.07 \cdot 10^{-2}$, $\Phi_0 = 0.336$, $\Phi_1 = 9.68 \cdot 10^{-2}$ ($\kappa = 0.356 < \kappa_3 = 0.71$ at $\alpha = 0.5$).

An example of a capture into resonant motion is presented in Fig. 3. Here we show the results of a computer integration of system (7). The initial conditions of the two trajectories differ only in the value of the angle φ. It is supposed that the comet is on an orbit similar to that of comet 2P/Encke, and its nucleus has two active zones. At the crossing of the hypersurface $\omega_\varphi = \omega_\psi$ we see a small deviation of Solution 1 from the corresponding solution of the averaged system. This is a manifestation of the phenomenon known as "scattering by a resonance". Solution 2 spends a long time near the resonant hypersurface.

Note that condition (15) is not formally valid in this case as $\varepsilon_* = 2.5$. Nevertheless, in nonresonant areas the solutions of the averaged equations are close to the solutions of the exact system.

For a detailed analysis of the solutions of Eqs. 7 when relations (22) take place, one can use the approach described in [2]. In Appendix B we show how to find the conditions for existence of solutions captured into the resonance $\omega_\varphi = 0$. Analogous conditions for the resonances $\omega_\varphi = \pm\omega_\psi$ and $2\omega_\varphi = \pm\omega_\psi$ are very tedious and, unfortunately, do not allow for any comprehensible interpretations. Either we have not analyzed the conditions of capture into resonances $\omega_\varphi = \pm 2\omega_\psi$. To make such a resonance possible, the nucleus would have to be strongly prolate ($c_* > \sqrt{5}a_*$, where a_* and c_* are small and the approximating ellipsoid has a long semi-major axis). Such a nucleus would, most probably, be torn into pieces by inertial forces.

5.Parameters in the averaged equations

It follows from Eqs. 14 that the parameters Φ_0 and Φ_1 in (13) are functions of the perihelion distance r_π and eccentricity e. Values of these functions for some values of r_π and e can be found in Tables II and III. In Table IV we present the values of Φ_0, Φ_1 for the comets mentioned in Table I.

At large values of the eccentricity ($e \approx 1$) one can use approximate formulas for Φ_0, Φ_1:

$$\Phi_0 \approx (1-e^2)^{3/2}\Psi_0(r_\pi)\,,\ \Phi_1 \approx (1-e^2)^{3/2}\Psi_1(r_\pi) \tag{23}$$

where

$$\Psi_0(r_\pi) = \frac{1}{\pi}\int_0^\pi g\left(\frac{2r_\pi}{1+\cos\nu}\right)\frac{d\nu}{(1+\cos\nu)^2} \tag{24}$$
$$\Psi_1(r_\pi) = \frac{1}{\pi}\int_0^\pi g\left(\frac{2r_\pi}{1+\cos\nu}\right)\frac{\cos\nu d\nu}{(1+\cos\nu)^2}$$

Table II. Values of $\Phi_0(r_\pi, e)$ at various orbit parameters.

	$e = 0.3$	$e = 0.5$	$e = 0.7$	$e = 0.9$	$e = 0.96$	$e = 0.99$
r_π=0.3	6.7100	3.6615	1.5027	0.2253	0.0542	0.0066
r_π=0.6	1.4930	0.7655	0.2658	0.0427	0.0104	0.0013
r_π=0.9	0.5747	0.2481	0.0898	0.0148	0.0036	0.0004
r_π=1.2	0.2426	0.0997	0.0376	0.0063	0.0015	0.0002
r_π=1.5	0.1002	0.0431	0.0165	0.0028	0.0007	0.0001

Table III. Values of $\Phi_1(r_\pi, e)$ at various orbit parameters.

	$e = 0.3$	$e = 0.5$	$e = 0.7$	$e = 0.9$	$e = 0.96$	$e = 0.99$
r_π=0.3	0.1559	0.1545	0.1437	0.0677	0.0182	0.0023
r_π=0.6	0.0468	0.0833	0.0913	0.0197	0.0050	0.0006
r_π=0.9	0.0491	0.0836	0.0461	0.0087	0.0022	0.0003
r_π=1.2	0.0588	0.0532	0.0241	0.0044	0.0011	0.0001
r_π=1.5	0.0462	0.0288	0.0122	0.0022	0.0005	0.0001

Table IV. Values of Φ_0, Φ_1 for some comets.

Comet	e	r_π	Φ_0	Φ_1
2P/Encke	0.846	0.341	0.336	0.097
46P/Wirtanen	0.652	1.063	0.068	0.039
1P/Halley	0.967	0.587	0.0084	0.0040
109P/Swift-Tuttle	0.9635	0.958	0.0026	0.0016

Note: In the table we used data from the website
`http://hssdc.gsfc.gov/planetary/factsheet/cometfact.html`.

Plots of the functions $\Psi_0(r_\pi)$ and $\Psi_1(r_\pi)$ are shown in Fig. 4a. For $r_\pi \gg 1\,A.U.$ the behavior of $\Psi_0(r_\pi), \Psi_1(r_\pi)$ can be described with asymptotic formulas

$$\Psi_0(r_\pi) \approx \frac{g_0}{4\sqrt{\pi}} \frac{\Gamma\left(c_1 + c_2 c_3 - \frac{3}{2}\right)}{\Gamma\left(c_1 + c_2 c_3 - 1\right)} \left(\frac{r_0}{r_\pi}\right)^{c_1 + c_2 c_3}, \tag{25}$$

$$\frac{\Psi_1(r_\pi)}{\Psi_0(r_\pi)} \approx \frac{c_1 + c_2 c_3 - 2}{c_1 + c_2 c_3 - 1} = 0.9594\ldots$$

where $\Gamma(\cdot)$ is the gamma function. If $r_\pi \ll 1\,A.U.$, analogous formulas have the form

$$\Psi_0(r_\pi) \approx \frac{g_0}{4\sqrt{\pi}} \frac{\Gamma\left(c_1 - \frac{3}{2}\right)}{\Gamma\left(c_1 - 1\right)} \left(\frac{r_0}{r_\pi}\right)^{c_1}, \tag{26}$$

$$\frac{\Psi_1(r_\pi)}{\Psi_0(r_\pi)} \approx \frac{c_1 - 2}{c_1 - 1} = 0.1301\ldots$$

The ratio $\Psi_1(r_\pi)/\Psi_0(r_\pi)$ monotonically increases as r_π grows (see Fig. 4b).

Parameters D_0, D_1, D_2 in Eqs. 13 represent integrals dependant on the properties of comet sublimation. If the nucleus shape is close to an axially symmetric ellipsoid, and the physical properties of its shape are mostly homogeneous (this is the model of continuously distributed mass ejection), the parameter values satisfy

$$|D_0| \sim |D_2| \ll |D_1|\,. \tag{27}$$

If, instead, mass ejection is localized over a small portion of the surface [21, 24], then

$$|D_0| \geq |D_1| \tag{28}$$

It should be pointed out, additionally, that the value of D_0/D_1 can vary strongly for the same comet shape as a function of how the active surface area is distributed on the nucleus. To better understand this variation we computed this ratio for a prolate ellipsoid approximated as a polyhedron with 4092 faces. To model the statistics of the ratio D_0/D_1 we made a series of Monte Carlo runs in which different portions of the surface were randomly chosen to be active (subject to a total active surface area constraint) and the ratio D_0/D_1 was computed for each case. The values of these ratios were stored for each distribution and the percentage which were greater than 1 was stored. For

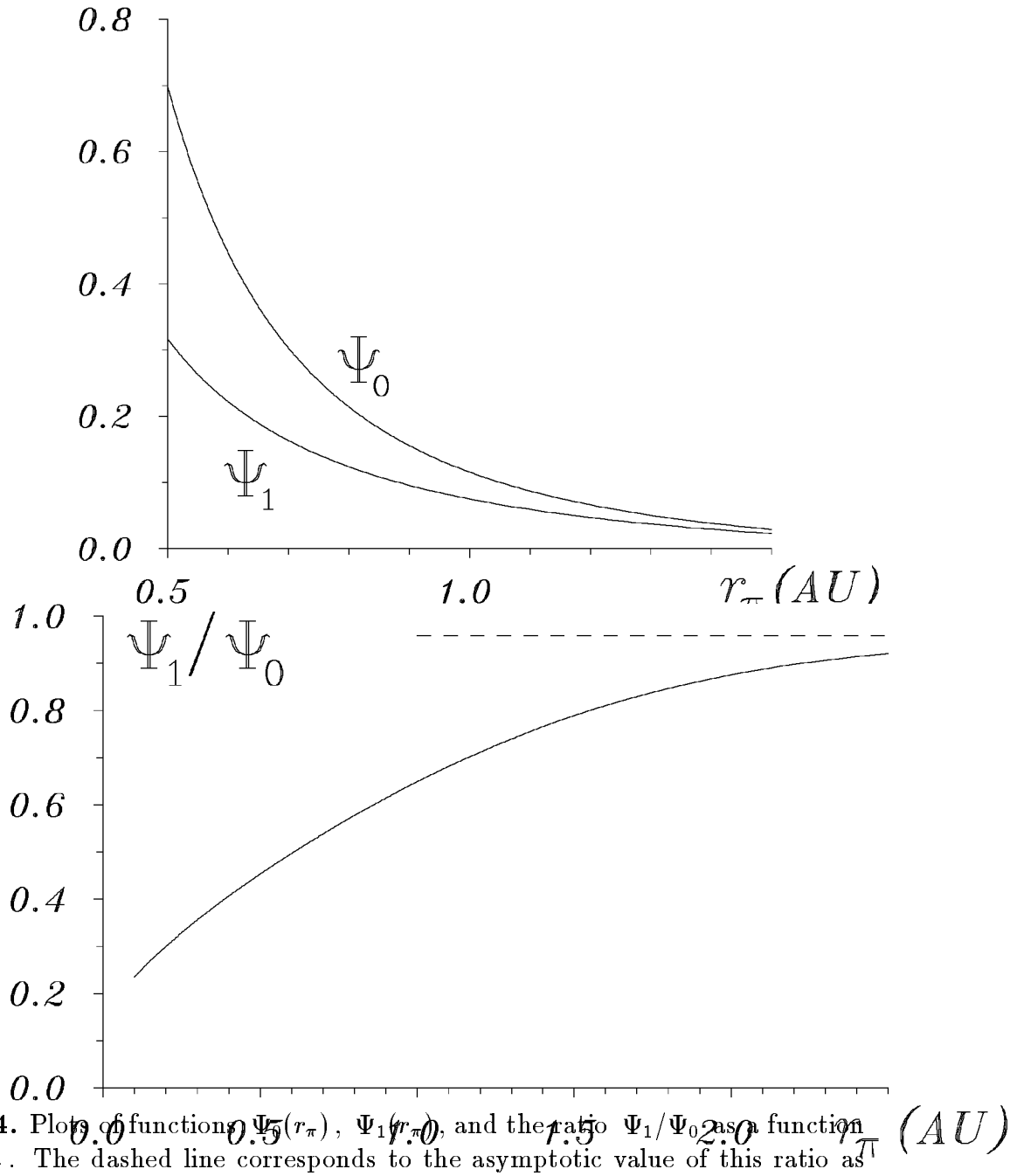

Fig.4. Plots of functions $\Psi_0(r_\pi)$, $\Psi_1(r_\pi)$, and the ratio Ψ_1/Ψ_0 as a function of r_π. The dashed line corresponds to the asymptotic value of this ratio as $r_\pi \to \infty$

these discretized prolate ellipsoids we found relatively constant percent of ratios greater than 1 for fractional area distributions less than 1, with ~ 90 percent of the possible active area distributions having a ratio greater than 1. For a uniformly active surface this percent drops to zero, and for a very small active area this percentage increases to 100. Figure 5 shows these statistics for a prolate ellipsoid with shape factor 3:1:1, and for comparison shows the similar curve computed for the "realistic" shape of asteroid Toutatis [9]. The same computations performed for other prolate ellipsoids yielded similar statistics. This clearly indicates that the constant distribution statistics are a function of the shape symmetry of a prolate ellipsoid, and that for a more realistic comet shape the statistics of this ratio would be more complex.

6.Discussion

Some general considerations of the evolution of nucleus rotation under reactive torques were made in [24]. Whenever the differences in the models used are not essential, our results are in good agreement with the results reported in [24] and obtained with numerical integrations of the nucleus equations of motion in the center of mass reference frame over long time intervals. In particular, the spinning up of the nucleus around the longitudinal axis described in [24] corresponds to the first scenario of evolution described in Section 4. We suppose that application of this averaging method to studies of the rotation of a nucleus with a nondegenerate inertia ellipsoid $(A_* > B_* > C_*)$ will result in other conditions that describe some of the other phenomena found in [24] (for example, spinning up of the nucleus around the axis with the largest principal moment of inertia.

Note that, according to modern ideas about the physical properties of the upper layer of a comet nuclei [6, 8, 17, 26], the empirical relation given in Section 2 is a very rough model of the real processes that occur. The realm of applicability of such relations is unknown in general. Nevertheless, it is remarkable that this simple model allows for a very detailed analysis of reactive torque effects on the nucleus spin evolution. Our results can be considered to be an indication of which physical parameters of the nucleus are relevant for its current state of rotation.

Application of the averaging method in studies of secular variations of rotation parameters is also useful when the mass ejection is described more accurately. Even when the averaged equations are too complicated for the analytical investigation, they still can simplify numerical studies at a basic level.

We can find several results of interest from the current analysis. First is the evolution of comet angular momentum as a function of time. As developed

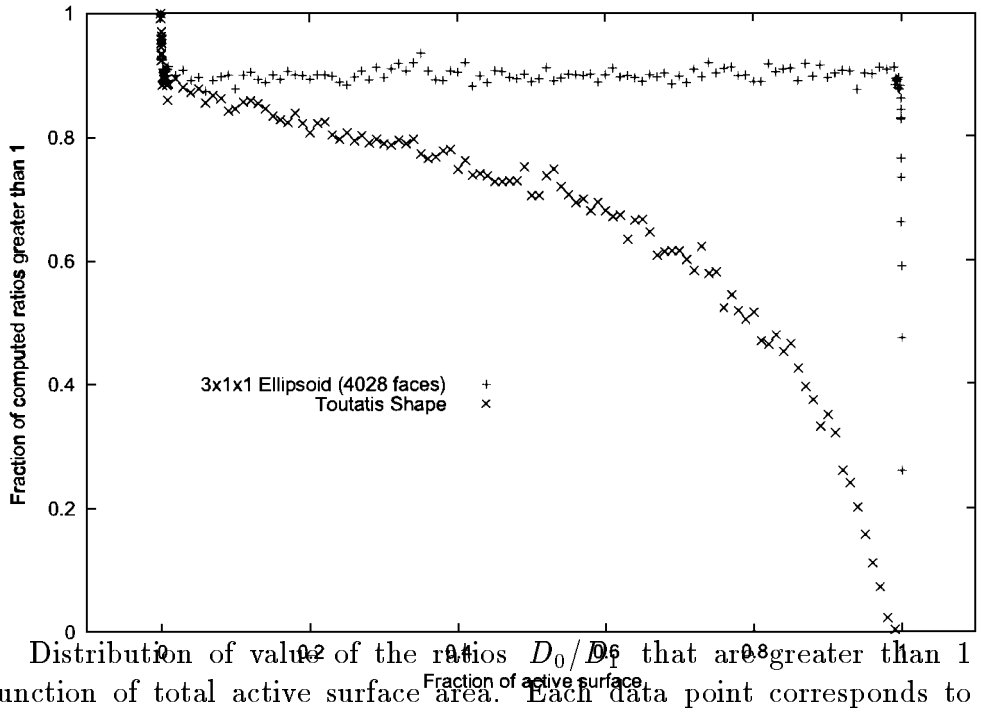

Fig.5. Distribution of value of the ratios D_0/D_1 that are greater than 1 as a function of total active surface area. Each data point corresponds to 1000 Monte Carlo runs generating a selection of possible ways in which the active surface areas can be distributed on the comet surface. The computation was performed for a discretized prolate ellipsoid and for the realistic Toutatis shape model. Note, the theory developed in the paper does not precisely fit with a shape model such as Toutatis', but the result is indicative of how the κ parameter may vary as a function of shape.

in Section 4 the ultimate trend in angular momentum is for it to increase as $L \sim \varepsilon c_o \tau$ for a rotating comet nucleus subject to reactive torques. The evolution of a comet nucleus under this asymptotic action implies that they will spin at increasing rates with time, which would naturally lead to the occasional splitting or bursting of a nucleus. Such comet splitting is seen relatively often, and is regarded as a natural occurence in the life of comets. The spin-up phenomenon identified here, in addition to other possible physical effects, would make such splitting a more common phenomenon by placing a comet nucleus under an increasing load with time.

Next is the relation between comet parameters and the final evolution of a comet nucleus. For non-resonant motion we find that the parameters of comet orbit, outgassing properties, and shape properties are combined into a single parameter κ that controls the evolution of the rotation state. Specifically, we recall that $\kappa = (D_0/D_1)\,(\Phi_0/\Phi_1)$, where the ratio Φ_0/Φ_1 depends only on the comet heliocentric orbit and the ratio D_0/D_1 is a function of the shape of the asteroid and its level of activity over the surface. While the orbital elements of comets are relatively well known, the actual shapes and surface activity of comet nuclei are not. Still, as mentioned previously it is reasonable to take an axis-symmetric, prolate body as an analogue for a comet shape. In terms of surface activity, there are a number of competing theories, which at their extremes would have the entire illuminated surface active or would have only a few isolated regions on the surface of a comet active.

We note that the ratio Φ_0/Φ_1 is greater than 1 for all our cases of interest. The magnitude of the ratio D_0/D_1 is not so easy to predict, however, and can take on different values depending on the body shape and the distribution of active regions over the surface. In Section 5 we make note that this ratio will be much less than 1 for a uniformly active surface, and should be strictly greater or equal to 1 for localized outgassing. These distinctions are important, as they lead to different definite values of the parameter κ. In particular, they indicate that a uniformly active surface may lead to values of κ near zero, which in general leads to a comet nucleus rotation state with nutation angle approaching $\sim 55^\circ$ and angular momentum cone angle approaching 90°. Conversely, a comet nucleus with only a few active surfaces should tend towards a zero nutation angle and a rotation pole aligned parallel to perihelion. Some indications of this mode were already found in [24]. We should note that their integrations were over limited time spans and had a slightly different outgassing torque formulation. Additionally, our current results are asymptotic, meaning that a comet nucleus angular momentum would tend towards these limits over long time spans. However, other phenomenon such as impacts, nucleus splitting, or close planetary flybys could disrupt this process and reset the nucleus rotational dynamics in a new state.

This aspect of the analysis does not give definite results for intermediate areas of the surface being active. It does give indications of the value of κ when the active surface area is very small (which corresponds to a large κ in all situations) and when the entire surface area is active (which corresponds to a small value of κ). For intermediate results we see that there will be a statistical element to the final result. We do have a clear indication, however, that the majority of cases will result in the rotational angular momentum of a comet to become parallel to its perihelion direction. Application of this analytical result to the analysis of comet light-curves may allow for an improved initial constraint to be placed on comet rotation poles.

7.Conclusions

A rigorous approach to the modeling of comet nucleus rotation in the presence of reactive sublimation torques is developed, analyzed, and applied to the rotational dynamics of comets. The approach averages over the rotational dynamics of the body and over the comet orbital motion about the sun. The inertia ellipsoid of the comet is assumed to be axially symmetric. The resulting dynamical system is time-invariant and can be characterized by a single parameter which combines information about the comet orbit with information about the comet shape and its outgassing surface activity. The main results of the analysis are that comets subject to outgassing torques will tend to gain angular momentum over time, and that the fraction of active surface area on a comet may lead to certain values of nutation angle and cause its angular momentum direction to align in specific directions related to its perihelion. More specifically, we show that the rotational angular momentum of comets with only a few active portions on their surface will tend to align with their orbit perihelion and spin about their minimum axis of inertia. Conversely, comets with uniformly active surfaces will tend to have a nutation angle of $\sim 55^\circ$ and have their angular momentum at a non-zero angle with perihelion.

Acknowledgements

This work was supported by the NASA JURRISS program under Grant NAG5-8715. AIN, AAV and VVS acknowledge support from Russian Foundation for Basic Research via Grants 00-01-00538 and 00-01-0174 respectively. DJS acknowledges support from the PG&G program via Grant NAG5-9017.

Appendix A. Effects of the postperihelion comet activity increase on nucleus spin evolution

To study the effects of possible activity growth after passing the perihelion we use, instead of (4), the formula

$$\widehat{g}(r,\nu) = g(r)(1+f(\nu)),$$

to describe the dependence of the mass ejection on the solar distance. Here $f(\nu)$ is an odd 2π-periodic function of ν positive over $\nu \in (0,\pi)$. Supposing that the activity asymmetry w.r.t. perihelion passage is small enough, we assume that $|f(\nu)| \ll 1$. We do not need the explicit expression for $f(\nu)$ in the following.

The evolution equations averaged over unperturbed nucleus motion around its mass center and over the orbit motion in this case have the form:

$$\frac{d\vartheta}{d\tau} = \frac{\varepsilon}{2L}[3\alpha D_1(\Phi_1 m_{Zz} + \Phi_2 m_{Xz})\cos\vartheta - 2(1-\alpha)\Phi_0 D_0]\sin\vartheta, \qquad (A1)$$

$$\frac{d\rho}{d\tau} = \frac{\varepsilon\alpha}{2L}[D_1(\Phi_1 m_{Zx} + \Phi_2 m_{Xx})R(\vartheta) + D_2\Phi_2 m_{Xy}\cos\vartheta],$$

$$\frac{d\sigma}{d\tau} = \frac{\varepsilon\alpha}{2L\sin\rho}[D_1 R(\vartheta) m_{Xy} - D_2(\Phi_1 m_{Zx} + \Phi_2 m_{Xx})\cos\vartheta],$$

$$\frac{dL}{d\tau} = -\varepsilon[\alpha D_1(\Phi_1 m_{Zz} + \Phi_2 m_{Xz})R(\vartheta) - (1-\alpha)D_0\Phi_0\cos\vartheta].$$

The physical sense of parameters $D_0, D_1, D_2, \Phi_0, \Phi_1$ was discussed in Section 5; Φ_2 is an integral parameter of the mass ejection asymmetry:

$$\Phi_2 = \frac{(1-e^2)^{3/2}}{\pi}\int_0^\pi \frac{\sin\nu g(r(\nu))f(\nu)d\nu}{(1+e\cos\nu)^2}. \qquad (A2)$$

As $g(r(\nu))$ is rapidly decreasing as ν grows (for typical values of orbit parameters e, r_π), the value of the integral in (A2) is determined by a small part of the integration interval, corresponding to a vicinity of the perihelion. Therefore,

$$0 < \Phi_2 \ll 1.$$

To describe the evolution of the angular momentum $\mathbf{L}$, introduce the auxiliary system of coordinatesт $O\widehat{X}\widehat{Y}\widehat{Z}$; this system is obtained by a turn of the perihelion system $OXYZ$ at the angle $\rho_* = \operatorname{arctg}\frac{\Phi_2}{\Phi_1}$ around the OY-axis. Orientation of the angular momentum vector w.r.t. trihedron $O\widehat{X}\widehat{Y}\widehat{Z}$ is

determined by the angles $\widehat{\rho}, \widehat{\sigma}$, like the angles ρ, σ determine its orientation w.r.t. trihedron $OXYZ$ (see Fig 1). Below are several relations between the angles $\widehat{\rho}, \widehat{\sigma}$ and ρ, σ:

$$\cos\widehat{\rho} = \cos\rho_* \cos\rho + \sin\rho_* \sin\rho\cos\sigma,$$

$$\sin\widehat{\rho}\cos\widehat{\sigma} = \cos\rho_* \sin\rho\cos\sigma - \sin\rho_*\cos\rho, \ \sin\widehat{\rho}\sin\widehat{\sigma} = \sin\rho\sin\sigma.$$

After changing the variables $(\rho, \sigma) \to (\widehat{\rho}, \widehat{\sigma})$ system (A1) can be written in the form:

$$\frac{d\vartheta}{d\tau} = \frac{\varepsilon}{2L}[3\alpha D_1\sqrt{\Phi_1^2+\Phi_2^2}\cos\widehat{\rho}\cos\vartheta - 2(1-\alpha)D_0\Phi_0]\sin\vartheta, \qquad (A3)$$

$$\frac{d\widehat{\rho}}{d\tau} = -\frac{\varepsilon\alpha\sin\widehat{\rho}}{4L}(2-3\sin^2\vartheta)D_1\sqrt{\Phi_1^2+\Phi_2^2}, \ \frac{d\widehat{\sigma}}{d\tau} = \frac{\varepsilon\alpha}{2L}\cos\vartheta D_2\sqrt{\Phi_1^2+\Phi_2^2},$$

$$\frac{dL}{d\tau} = -\frac{\varepsilon}{2}[\alpha D_1\sqrt{\Phi_1^2+\Phi_2^2}(2-3\sin^2\vartheta)\cos\widehat{\rho} - 2(1-\alpha)D_0\Phi_0\cos\vartheta].$$

Except for the notations, system (A3) is similar to system (13). Thus, small asymmetries in mass ejection rates do not significantly affect the scenarios of nucleus rotation evolution considered in Section 4. The main difference is that, when describing the orientation of the angular momentum vector at $\tau \to \infty$, one should use the direction of the nucleus radius-vector at $\nu = \rho_*$ instead of the direction from the Sun to the perihelion.

Appendix B. Resonance at $\omega_\varphi \approx 0$.

As mentioned in Section 3, this resonance is found for those motions where the longest axis of the nucleus is perpendicular to the angular momentum vector $\mathbf{L}$ $\left(\vartheta \approx \frac{\pi}{2}\right)$.

To study phenomena occuring at the resonance $\omega_\varphi = 0$, we introduce in (7) a new variable $q = \omega_\varphi$ instead of ϑ. This new variable describes deviations from the resonant surface. We average the r.h.s. of the equations for slow variables ρ, σ, L over the nonperturbed nucleus motion and over the orbital motion. We do the same averaging also in the equation for q, which is a "semi-fast" variable in a $\sqrt{\varepsilon}$-neighborhood of the resonant surface $\omega_\varphi = 0$ (i.e. $d\varphi/d\tau \sim \sqrt{\varepsilon}$). Note, that averaging over the nucleus motion in this case is averaging over the fast variable ψ. Changing the variables $(\tau, q) \to (\upsilon, \chi)$, where $\upsilon = \sqrt{\varepsilon}\tau$ and $\chi = q/\sqrt{\varepsilon}$ we rewrite the system in the "pendulum-like" form:

$$\frac{d\rho}{dv} = \sqrt{\varepsilon}K_\rho(\rho, L, \chi, \varphi, \varepsilon),\ \frac{d\sigma}{dv} = \sqrt{\varepsilon}K_\sigma(\rho, L, \chi, \varphi, \varepsilon), \qquad (B1)$$

$$\frac{dL}{dv} = \sqrt{\varepsilon}K_L(\rho, L, \chi, \varphi, \varepsilon),\ \frac{d\varphi}{dv} = \chi + \sqrt{\varepsilon}K_\varphi(\rho, L, \chi, \varphi, \varepsilon),$$

$$\frac{d\chi}{dv} = \Xi(\rho, \varphi) + \sqrt{\varepsilon}K_\chi(\rho, L, \chi, \varphi, \varepsilon).$$

The explicit expression for $\Xi(\rho, \phi)$ in (B1) is:

$$\Xi(\rho, \varphi) = \Xi_0 + \Xi_1 \sin(\varphi + \varphi_\chi),$$

$$\Xi_0 = (1 - \alpha)\left(\frac{1}{C} - \frac{1}{A}\right)\Phi_0 D_0,$$

$$\Xi_1(\rho) = \alpha\Phi_1|\cos\rho|\left(\frac{1}{C} - \frac{1}{A}\right)\sqrt{(D_1^\xi)^2 + (D_1^\eta)^2},$$

$$\varphi_\chi = \frac{\pi}{2}\left[1 - \text{sign}\left(\cos\rho D_1^\xi\right)\right] + \text{arctg}\left(\frac{D_1^\eta}{D_1^\xi}\right),$$

$$D_1^\xi = \sum_{j=1}^{N} s_j d_{j\zeta} n_{j\xi},\ D_1^\eta = \sum_{j=1}^{N} s_j d_{j\zeta} n_{j\eta}.$$

We do not need the expressions for $K_\rho, K_\sigma, K_L, K_\chi, K_\varphi$ in the following considerations.

At $\varepsilon = 0$ in (B1) the closed subsystem arises:

$$\frac{d\varphi}{dv} = \chi\,,\ \frac{d\chi}{dv} = \Xi_0 + \Xi_1(\rho)\sin(\varphi + \varphi_\chi)\,, \qquad (B2)$$

This subsystem coincides with equations of motion of a pendulum under the a constant torque (variable ρ in (B2) is a parameter). If $|\Xi_0| > \Xi_1$, the "pendulum" rotates, and the velocity of the rotation either monotonically grows or monotonically decreases depending on the sign of Ξ_0. In this case, capture of solutions of the original system (7) into the resonance $\omega_\varphi = 0$ is not possible.

If $|\Xi_0| < \Xi_1$, the system (B2) possesses oscillatory solutions. This implies existence of resonant motions of the comet nucleus, such that $\omega_\varphi \approx 0$ for a long time. Denote the set of values of the angle ρ that satisfy the condition $|\Xi_0| < \Xi_1(\rho)$ as $\mathcal{D}_0$.

At $\varepsilon \neq 0$, projections of some phase trajectories of (B1) onto the plane (χ, φ) cross the separatrix of the phase portrait of the pendulum-like system (B2). Trajectories entering the oscillatory domain correspond to the solutions of (7) captured into the resonance. Exit from the oscillatory domain corresponds to escape from the resonance.

Like the original system (7), system (B1) is reversible: if

$$(\rho(v), \sigma(v), L(v), \varphi(v), \chi(v)) \qquad (B3)$$

is a solution, then

$$(\pi - \rho(-v), \pi + \sigma(-v), L(-v), \pi + \varphi(-v), -\chi(-v)) \qquad (B4)$$

is also a solution. Projections of the phase trajectories (B3) and (B4) onto the plane (φ, χ) cross the separatrices of (B2) in opposite directions. Hence, solutions of (7) captured into the resonance $\omega_\varphi = 0$ can be found among those reaching the resonant surface when $\rho = \rho^* \in \mathcal{D}_0$, or among those reaching it when $\rho = \pi - \rho^*$. Capture into this resonance are impossible only if $\mathcal{D}_0 = \emptyset$. One can show, using the expressions for Ξ_0 and Ξ_1, that $\mathcal{D}_0 \neq \emptyset$ if

$$(1 - \alpha)\Phi_0 D_0 < \alpha\Phi_1 \sqrt{(D_1^\xi)^2 + (D_1^\eta)^2}. \qquad (B5)$$

Inequality (B5) is certainly violated if mass ejection is localized on a small spot of the nucleus surface. Indeed, if $N = 1$, we find

$$(D_1^\xi)^2 + (D_1^\eta)^2 = D_0^2 - D_1^2 .$$

At any initial conditions, the rotational evolution of such a nucleus evolves without being captured into the resonance $\omega_\varphi = 0$.

References

[1] V.I.Arnold *Mathematical methods of classical mechanics.* Springer, New York, 1978.

[2] V.I.Arnold, V.V.Kozlov, and A.I.Neishtadt, *Mathematical aspects of classical and celestial mechanics (Encyclopaedia of mathematical sciences 3)* (Springer, Berlin, 1988).

[3] V.V.Beletsky, Motion of a satellite around its mass center. Moscow, 1965 (in Russian)

[4] N.N.Bogolyubov and Yu.A.Mitropolsky *Asymptotic Methods in the Theory of Nonlinear Oscillations* (New York: Gordon and Breach Science Publ. **537**, 1961)

[5] J.A. Burns, V. Safronov, Asteroid nutation angles.
MNRAS. 1973. V. 165. P. 403.

[6] J.F.Crifo, A.V.Rodionov, Modelling the circumnuclear coma of comets: objectives, methods and recent results
Planetary and Space Science. 1999. V. 47. N 6–7. P. 797–826.

[7] M.Efroimsky, A.Lazarian, Inelastic dissipation in wobbling asteroids and comets
MNRAS. 2000. V. 311. N 1. P. 269.

[8] M.C.Festou, H.Rickman, R.M.West, Comets
ESO Preprint. 1993. N 960.

[9] R.S. Hudson and S.J. Ostro, Shape and non-principal axis spin state of asteroid 4179 Toutatis, Science 270, 84–86, 1995.

[10] V.V.Ivashkin, M.Bello Moro, Cometary activity model for near nucleus space flight dynamics analysis
Proceedings of the 12th international symposium on space flight dynamics, held in Darmstadt, Germany. 1997. P. 335–340.

[11] D.C.Jewitt, K.J.Meech, Optical properties of cometary nuclei and a preliminary comparison with asteroids
Astrophys. J. 1988. V. 328. P. 974–986

[12] L.Jorda, J.Licandro, Modeling the rotation of comets
Proceedings of the IAU Colloquim 168, held in Nanjing, China. Pub. Astron. Soc. Pacific (in press).

[13] W.H.Julian, Precession of triaxial cometary nuclei
Icarus. 1988. V. 74. P. 377–382.

[14] Lars Kamél, The evolution of P/Encke's light curve: no secular fading, a vanishing perihelion asymmetry
Icarus. 1991. V. 93. P. 226–245.

[15] H.U.Keller, W.A.Delamere, W.F.Huebner, H.J.Reitsema, H.U.Schmidt, F.L.Whipple, K.Wilhelm, W.Curdt, R.Kramm, N.Thomas, C.Arpigny, C.Barbieri, R.M.Bonnet, S.Cazes, M.Coradini, C.B.Cosmovici, D.W.Hughes, C.Jamar, D.Malaise, K.Schmidt, W.K.H.Schmidt, P.Seige, Comet P/Halley's nucleus and its activity
Astron. Astrophys. 1987. V. 187. P. 807–823.

[16] M.M.Komarov, V.V.Sazonov, Calculation of light pressure forces and torques on an asteroid of arbitrary shape, Astron.Vestn., v.28, No.1, pp.21-30, 1994 (in Russian)

[17] M.Ya.Marov, Physical properties and models of comets, Astron. Vestn., v.28, No.4-5, 1994 (in Russian)

[18] B.G.Marsden, Z.Sekanina, D.K.Yeomans, Comets and nongravitational forces.V
Astron. J. 1973. V. 78. P. 211–225.

[19] L.A.McFadden, The comet-asteroid transition: recent telescopic observations
Asteroids, comets, meteors 1993 / Eds A.Milane et al. Dordrecht: Kluwer. 1994. P. 95–110.

[20] Yu.D.Medvedev, On formation of elongated cometary nuclei
Proceedings of the second international workshop on positional astronomy and celestial mechanics held in Valencia, Spain/ Eds A.Lopez Garcia et al. 1993. P. 63–80.

[21] S.J.Peale, J.J.Lissauer, Rotation of Halley's comet
Icarus. 1989. V. 79. P. 396–430.

[22] R.Z.Sagdeev, K.Szego, B.A.Smith, S.Larson, E.Merenyi, A.Kondor, I.Toth, The rotation of P/Halley
Astron. J. 1989. V. 97. N 2. P. 546–551.

[23] N.H.Samarasinha, M.F.A'Hearn, Observational and dynamical constraints on the rotation of comet P/Halley
Icarus. 1991. V. 93. P. 194–225.

[24] N.H.Samarasinha, M.J.S.Belton, Long-term evolution of rotational states and nongravitational effects for Halley-like cometary nuclei
Icarus. 1995. V. 116. P. 340–358.

[25] D.J.Scheeres, F.Marzari, L.Tomasella, V.Vanzani, ROSETTA mission: satellite orbits around a cometary nucleus
Planetary Space Sci., 1998. V. 46. P. 649–671.

[26] L.I.Shulman, Comet nuclei. Moscow, 1987 (in Russian)

[27] J.Watanabe, Rotational motion of the nucleus of comet P/Halley
Publ. Astron. Soc. Japan, 1989. V. 41. P. 897–918.

[28] C.J.Weeks, The effect of comet outgassing and dust emission on the navigation of an orbiting spacecraft
J. Astronaut. Sci., 1995. V. 43. N 3. P. 327–343.

[29] F.L.Whipple, Z.Sekanina, Comet Encke: precession of the spin axis, nongravitational motion and sublimation
Astron. J., 1979, V. 84. P. 1894–1909.

[30] F.L.Whipple, The rotation of comet nuclei
Comets/Ed. Wilkening E.L. Tucson: Arizona Press, 1982, P. 227–250.

[31] K.Wilhelm, Rotation and precession of comet Halley
Nature. 1987. V. 327. P. 27–30.

[32] D.K.Yeomans, P.W.Chodas, An asymmetric outgassing model for cometary nongravitational accelerations
Astron. J. 1989. V. 98. N 3. P. 1083–1093.